Naval Research Laboratory

Washington, DC 20375-5320

NRL/MR/7140--99-8385

Target Detection Using a Linear Sum of Matched Filter Outputs

DAVID M. DRUMHELLER

Acoustic Systems Branch
Acoustics Division

HENRY LEW

Defence Science and Technology Organisation
Maritime Operations Division
Salisbury, SA 5108, Australia

June 30, 1999

REPORT DOCUMENTATION PAGE

Form Approved
OMB No. 0704-0188

1. AGENCY USE ONLY (*Leave Blank*)	2. REPORT DATE	3. REPORT TYPE AND DATES COVERED
	June 30, 1999	Final

4. TITLE AND SUBTITLE

Target Detection Using a Linear Sum of Matched filter Outputs

5. FUNDING NUMBERS

PE-0602314N

6. AUTHOR(S)

David M. Drumheller and Henry Lew*

7. PERFORMING ORGANIZATION NAME(S) AND ADDRESS(ES)

Naval Research Laboratory
Washington, DC 20375-5320

8. PERFORMING ORGANIZATION REPORT NUMBER

NRL/MR/7140--99-8385

9. SPONSORING/MONITORING AGENCY NAME(S) AND ADDRESS(ES)

Office of Naval Research
Code 321US
Arlington, VA 22217-5660

10. SPONSORING/MONITORING AGENCY REPORT NUMBER

11. SUPPLEMENTARY NOTES

* Defence Science and Technology Organisation
Maritime Operations Division
Salisbury, SA 5108, Australia

12a. DISTRIBUTION/AVAILABILITY STATEMENT

Approved for public release; distribution is unlimited.

12b. DISTRIBUTION CODE

13. ABSTRACT (*Maximum 200 words*)

Mathematical techniques are presented for deriving approximations to the statistical functions that characterize linear sums of matched filter outputs. The approximations are derived using two techniques: (i) Padé approximations to the multi-dimensional characteristic function and (ii) discrete Rayleigh mixtures based on an exact or approximate form of the echo power probability density function. It is also shown how these two techniques are related to each other mathematically.

14. SUBJECT TERMS

Detection theory	Probability of false alarm	Target fluctuation model
Radar	Multiple observations	Clutter fluctuation model
Sonar	Non-Gaussian	Padé approximation
Probability of detection	Mixture model	

15. NUMBER OF PAGES

34

16. PRICE CODE

17. SECURITY CLASSIFICATION OF REPORT	18. SECURITY CLASSIFICATION OF THIS PAGE	19. SECURITY CLASSIFICATION OF ABSTRACT	20. LIMITATION OF ABSTRACT
UNCLASSIFIED	UNCLASSIFIED	UNCLASSIFIED	UL

NSN 7540-01-280-5500

Standard Form 298 (Rev. 2-89)
Prescribed by ANSI Std 239-18
298-102

CONTENTS

Target Detection Using a Linear Sum of Matched Filter Outputs

1. INTRODUCTION

The matched filter is the most common receiver structure used for target detection in echolocation systems. As shown in Figure 1, it is composed of a multiplier that combines the received echo, $s(t)$, and the processing waveform, $g(t - T_d)$, where T_d is the range delay. This is followed by an integrator. Since the processing signal is a function of range delay[1], the complex matched filter output, y, is also a function of range delay and is sampled in time to form "bins." The amplitude of the resulting complex value in each bin, the "detection statistic," is compared to a threshold. When the statistic exceeds the threshold, a detection is declared.

The above detection scheme is based on only one bin value at a fixed range being available during a single ping cycle, and is thus referred to as "single-observation detection." In some cases, multiple observations are available because, for example, an echo may be divided into subbands (in frequency) that are separately processed (matched filtered). When several observations are simultaneously available, they can (or should) be used collectively to determine if a target is present. This can be accomplished by using a more general form of the matched filter where the observations, each originating from a separate matched filter, are summed to form a single detection statistic.

This report documents mathematical techniques for approximating the probability density function (PDF) and other statistical functions that characterize matched filter outputs and detection statistics that are a linear combination of the outputs. The approximations can be used for computing detection thresholds and detection probabilities as a function of signal-to-clutter ratio (SCR). The approximations are either based on Padé approximations to the multi-dimensional characteristic function (CF), or are discrete mixtures based on an exact or approximate form of the Rayleigh mixture parameter (echo power) PDF.

This report documents mathematical techniques for determining the probability of detection, P_d, and detection threshold, γ, for a given probability of false alarm, P_{fa}, when using either a single output or a linear sum of multiple outputs of a matched filter. This includes techniques for modeling the statistical nature of the matched filter response to target and clutter echoes. Specific results include the following:

- Recently reported techniques for approximating the statistical functions that model a single matched filter output and are based on Padé approximations to the CF are extended to multiple observations (Section 3.5).
- Techniques were developed that yield accurate, discrete Rayleigh mixture models of multidimensional PDFs and related statistical functions (Sections 2.5 and 3.6).

Manuscript approved June 16, 1999.

[1]More generally, the processing signal can also be a function of other variables such as Doppler and bearing.

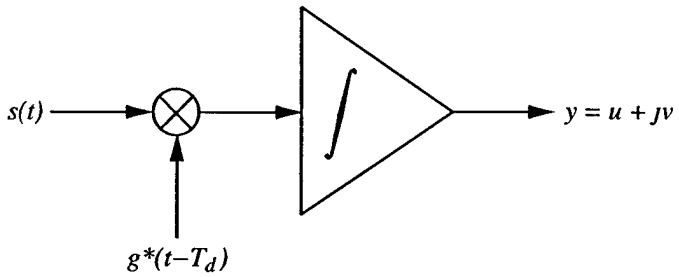

Fig. 1 – The matched filter.

- The aforementioned Padé-based techniques have been extended to include approximations to the statistical functions that model the Rayleigh mixture parameter (Section 2.4).
- It was found that Padé-based approximations are best suited for approximating the "tails" of the PDFs, and thus may be used to determine the detection threshold given a specific false alarm probability where typically $P_{fa} < 0.001$ (Section 3.5).
- It was found that approximations based on mixture models are best suited for approximating the "peaks" of the PDFs, and thus may be used to determine target detection probabilities where typically $0.1 < P_d < 0.9$ (Sections 2.5 and 3.10).

Unlike other treatments of the detection problem where the target is assumed to be "steady," it is assumed here that a matched filter output fluctuates in response to the target echo. This is true in echolocation systems (especially sonar systems operating in "search mode") where the range resolution is equal to or larger than the line-of-sight target size.

To summarize, this report is organized into two main sections: (i) modeling a single observation and (ii) modeling multiple observations. The first section provides the necessary background from which detection using multiple observations is developed. It begins with a summary of the underlying assumptions of the single-observation detection problem for echolocation systems. This leads to a discussion of the CF and Rayleigh mixture model representations and their corresponding approximations for the matched filter output statistical functions. Examples of both Rayleigh and non-Rayleigh fluctuation models are used to illustrate the techniques. The second section then builds on these results to account for multiple observations by developing techniques to approximate multivariate statistical functions. It includes a description of the receiver structure and the associated calculations of the detection threshold and probability of detection. Examples of receiver operating characteristic curves conclude the section.

2. BACKGROUND: MODELING A SINGLE OBSERVATION

2.1 Statistical Assumptions

Suppose the complex output of a matched filter receiver is given by

$$y = u + jv = re^{j\theta} \tag{1}$$

where r and θ are respectively the amplitude and phase of the matched filter output. Under the common assumption that there is no knowledge of its likely value, the phase is modeled as a uniform random variable in the interval $[0, 2\pi)$. This implies that u and v are zero-mean random variables

and their joint PDF is circularly symmetric. Using the polar notation (r, θ), this joint PDF has the following form:

$$f_{U,V}(u,v) = f_{R,\Theta}(r,\theta) = \frac{f_R(r)}{2\pi r} \tag{2}$$

where $f_R(r)$ is the PDF of the amplitude r. The CF for u and v is equal to the two-dimensional Fourier transform of the joint PDF in (2) and is denoted as $\Phi(\omega, \xi)$. It is possible to show that due to the circular symmetry of the joint PDF, the CF is also circularly symmetric and is only a function of the "radial frequency," $\rho = \sqrt{\omega^2 + \xi^2}$. Consequently, only the relationship between the CF and the amplitude PDF is important and is expressed by the following Hankel transform pair [10]:

$$\Phi(\rho) = \int_0^\infty f_R(r) J_0(\rho r)\, dr \tag{3}$$

$$f_R(r) = r \int_0^\infty \rho \Phi(\rho) J_0(\rho r)\, d\rho \tag{4}$$

where $J_0(\cdot)$ is the zeroth-order Bessel function of the first kind. Detection probabilities are given by the survival function (SF), defined as

$$S_R(r) = \int_r^\infty f_R(t)\, dt. \tag{5}$$

2.2 The Rayleigh Mixture Amplitude Fluctuation Model

The Rayleigh mixture amplitude fluctuation model is defined as

$$f_R(r) = r \int_0^\infty \frac{1}{\tau} \exp\left(-\frac{r^2}{2\tau}\right) f_\tau(\tau)\, d\tau \tag{6}$$

where $f_\tau(\tau)$ is the PDF of the Rayleigh parameter, τ, and is referred to as the "characteristic PDF." Integration and Hankel transformation of (6) leads to

$$S_R(r) = \int_0^\infty \exp\left(-\frac{r^2}{2\tau}\right) f_\tau(\tau)\, d\tau \tag{7}$$

$$\Phi(\rho) = \int_0^\infty \exp\left(-\frac{\tau\rho^2}{2}\right) f_\tau(\tau)\, d\tau. \tag{8}$$

This model was deduced from the observation that some radar clutter appears to exhibit Rayleigh statistics whose power is dependent upon the portion of the environment being observed [16]. One PDF that has been successfully employed as a radar clutter model is the K-type PDF, which can be shown to be a Rayleigh mixture whose characteristic PDF is a gamma distribution. Anecdotal evidence suggests that acoustic scattering from the ocean floor may also follow a K-type PDF, thus suggesting that Rayleigh mixture models might be employed as sonar reverberation models[2].

[2]This is a result of data analysis performed by the authors. References on this work are not currently available.

2.3 Approximate Amplitude Fluctuation Models Based on Padé Approximations

It is shown in References 5 and 6 that the CF may be approximated by a Padé approximation (rational approximation):

$$\Phi(\rho) \approx \frac{1 + a_1\rho^2 + a_2\rho^4 + \ldots a_L\rho^{2L}}{1 + b_1\rho^2 + b_2\rho^4 + \ldots b_M\rho^{2M}} \tag{9}$$

where $L < M$. The coefficients of the numerator and denominator of (9) can be found from the amplitude PDF by either "moment matching" at the origin ($\rho = 0$) or by "interpolation." In the case of moment matching, the denominator coefficients are found first by solving the matrix equation

$$\begin{pmatrix} c_{L-M+1} & c_{L-M+2} & \cdots & c_L \\ c_{L-M+2} & c_{L-M+3} & \cdots & c_{L+1} \\ \vdots & \vdots & & \vdots \\ c_L & c_{L+1} & \cdots & c_{L+M-1} \end{pmatrix} \begin{pmatrix} b_M \\ b_{M-1} \\ \vdots \\ b_1 \end{pmatrix} = \begin{pmatrix} -c_{L+1} \\ -c_{L+2} \\ \vdots \\ -c_{L+M} \end{pmatrix} \tag{10}$$

where $c_0 = 1$, $c_k = 0$ for $k < 0$ and

$$c_k = \frac{(-1)^k E\{r^{2k}\}}{(k!)^2\, 2^{2k}} \quad \text{for } k > 0 \tag{11}$$

with $E\{r^{2k}\}$ denoting the $2k$-th moment of the amplitude PDF. Once $b_1, \ldots, b_M$ have been found, the numerator coefficients can be determined using

$$a_i = b_i + c_i + \sum_{k=1}^{i-1} b_{i-k} c_k \quad \text{for } i = 1, \ldots, L. \tag{12}$$

The Padé approximation in (9) can be written as a partial fraction expansion:

$$\Phi(\rho) \approx \sum_{k=1}^{M} \frac{A_k}{(\rho^2 - p_k)^{m_k}}. \tag{13}$$

Treating the CF as a Hankel transform and inverting the partial fraction expansion in (13) yields an approximation for the amplitude PDF:

$$f_R(r) \approx \sum_{k=1}^{M} \frac{A_k r^{m_k} K_{m_k-1}(\sqrt{-p_k}\, r)}{(2\sqrt{-p_k})^{m_k-1}(m_k - 1)!}. \tag{14}$$

Integration of (14) yields an approximation for the SF:

$$S_R(r) \approx \sum_{k=1}^{M} \frac{2A_k r^{m_k} K_{m_k}(\sqrt{-p_k}\, r)}{(2\sqrt{-p_k})^{m_k}(m_k - 1)!}. \tag{15}$$

2.4 Approximate Rayleigh Parameter Fluctuation Models Based on Padé Approximations

A Padé approximation to the CF can also be used to derive an approximation to the characteristic PDF and its associated SF. These approximations are

$$f_\tau(\tau) \approx \sum_{k=1}^{M} \frac{A_k}{2^{m_k}\Gamma(m_k)}\,\tau^{m_k-1}\exp\left(\frac{p_k\tau}{2}\right) \tag{16}$$

$$S_\tau(\tau) \approx \sum_{k=1}^{M} \frac{A_k}{(-p_k)^{m_k}\Gamma(m_k)}\,\Gamma\left(m_k, -\frac{p_k\tau}{2}\right) \tag{17}$$

where $\Gamma(n,t)$ denotes the incomplete gamma function. The approximation in (16) may be verified by substituting it into (8) and carrying out the elementary integration to get (13). The approximation in (17) follows from the integration of (16). If $m_k = 1$ for all k (which is usually the case), then (17) reduces to

$$S_\tau(\tau) \approx -\sum_{k=1}^{M} \frac{A_k}{p_k}\exp\left(\frac{p_k\tau}{2}\right). \tag{18}$$

These equations are valid only when $\mathrm{Re}\{p_k\} < 0$ for all k, since this condition implies that the terms in (16) and (17) will eventually decay to zero as the Rayleigh parameter becomes large[3]. In the following examples, the Nakagami, K-type and Rayleigh fluctuation models are used to illustrate the accuracy of (16) and (17) by comparing them to their known analytic forms.

The Nakagami Target Fluctuation Model

Consider the example of a Nakagami target fluctuation model given by:

$$f_R(r) = \frac{N^N r^{2N-1}}{2^{N-1}\Gamma(N)\sigma^{2N}} e^{-Nr^2/(2\sigma^2)} \tag{19}$$

$$S_R(r) = \frac{1}{\Gamma(N)}\Gamma\left(N, \frac{Nr^2}{2\sigma^2}\right) \tag{20}$$

$$\Phi(\rho) = 1 + \sum_{k=1}^{\infty} \frac{(-1)^k N(N+1)\ldots(N+k-1)}{(k!)^2}\left(\frac{\sigma^2\rho^2}{2N}\right)^k. \tag{21}$$

This fluctuation model follows from the chi-square model for target strength (r^2) [12,7]. In particular, $N = 1$ corresponds to a Rayleigh model and $N = 2$ corresponds to a one-dominant-plus-Rayleigh model [4]. For $N < 1$, the characteristic PDF for this model is given by [14]

$$f_\tau(\tau) = \begin{cases} \left(\dfrac{N}{\sigma^2}\right)^N \dfrac{\tau^{N-1}}{\Gamma(N)} \displaystyle\sum_{i=0}^{\infty} \frac{(-N\tau/\sigma^2)^i}{\Gamma(i+1)\Gamma(1-N-i)} & \text{for } 0 < \tau < \sigma^2/N \\ 0 & \text{for } \sigma^2/N \le \tau. \end{cases} \tag{22}$$

[3]It is shown in Reference 5 that for the Hankel transform to be "stable," which results in approximations to the amplitude PDF and SF that decay to zero as $r \to \infty$, the poles (p_k for $k = 1 \ldots M$) cannot be positive real numbers. This admits the possibility of complex poles with positive real parts and non-zero imaginary parts. Such poles would not yield approximations to the characteristic PDF and SF that decay to zero as $\tau \to \infty$. Nevertheless, it has been the authors' experience that poles for Padé-based approximations to the amplitude PDFs and SFs for models that are known to be Rayleigh mixtures (e.g., the Weibull, Nakagami and K-type models) have negative real parts.

The exact form of the characteristic SF is obtained by integration of (22) and is given by

$$S_\tau(\tau) = \begin{cases} \left(\frac{N}{\sigma^2}\right)^N \frac{\tau^N}{\Gamma(N)} \sum_{i=0}^{\infty} \frac{(-N\tau/\sigma^2)^i}{(N+i)\Gamma(i+1)\Gamma(1-N-i)} & \text{for } 0 < \tau < \sigma^2/N \\ 0 & \text{for } \sigma^2/N \le \tau. \end{cases} \tag{23}$$

For $N = 0.5$ and $\sigma^2 = 1$, it is shown in Reference 5 that

$$\begin{aligned} \Phi(\rho) \approx & \frac{-19.78778 + \jmath 258.7502}{\rho^2 + 7.782720 + \jmath 1.618012} + \frac{-19.78778 - \jmath 258.7502}{\rho^2 + 7.782720 - \jmath 1.618012} \\ & + \frac{30.66573 - \jmath 102.2120}{\rho^2 + 6.813219 + \jmath 4.909758} + \frac{30.66573 + \jmath 102.2120}{\rho^2 + 6.813219 - \jmath 4.909758} \\ & + \frac{-8.790265 + \jmath 9.696267}{\rho^2 + 4.478996 + \jmath 8.421761} + \frac{-8.790265 - \jmath 9.696267}{\rho^2 + 4.478996 - \jmath 8.421761}. \end{aligned} \tag{24}$$

Substituting the coefficients and poles of the partial fraction expansion in (24) into (16) and (17) and carrying out the tedious algebra yields

$$\begin{aligned} f_\tau(\tau) \approx & 259.5057 \exp(-3.891360\tau) \cos(0.809006\tau - 1.647122) \\ & + 106.7131 \exp(-3.406610\tau) \cos(2.454879\tau + 1.279320) \\ & + 13.08764 \exp(-2.239498\tau) \cos(4.210881\tau - 2.307225) \end{aligned} \tag{25}$$

$$\begin{aligned} S_\tau(\tau) \approx & 65.29159 \exp(-3.891360\tau) \cos(0.809006\tau - 1.442144) \\ & + 25.41406 \exp(-3.406610\tau) \cos(2.454879\tau + 1.903753) \\ & + 2.744104 \exp(-2.239498\tau) \cos(4.210881\tau - 1.225219). \end{aligned} \tag{26}$$

The exact forms and approximations to the characteristic PDF and SF are shown in Figures 2 and 3. Figure 3 reveal that (26) is a respectable approximation to the characteristic SF that deviates about the exact form. This modeling error is reflected by the more obvious deviations seen in the approximation to the characteristic PDF. Figure 4 shows the relative errors between the exact form of the characteristic PDF and SF and their approximations, and are defined by

$$\text{RE} = \log_{10}\left|1 - \frac{\text{approximate equation}}{\text{exact equation}}\right|. \tag{27}$$

The negative value of the relative error is approximately equal to the number of significant digits of agreement between the exact equation and its approximation. Generally, an approximation is considered good when RE ≤ -2. For Figure 4 the relative error was not calculated for $\tau > 2$ because the exact form is identically zero for this interval.

The K-type Clutter Fluctuation Model

As another example, consider the K-type clutter fluctuation model given by

$$f_R(r) = \frac{2b}{\Gamma(\nu+1)} \left(\frac{br}{2}\right)^{\nu+1} K_\nu(br) \tag{28}$$

$$S_R(r) = \frac{2}{\Gamma(\nu+1)} \left(\frac{br}{2}\right)^{\nu+1} K_{\nu+1}(br) \tag{29}$$

$$\Phi(\rho) = \frac{1}{[1 + (\rho/b)^2]^{\nu+1}}. \tag{30}$$

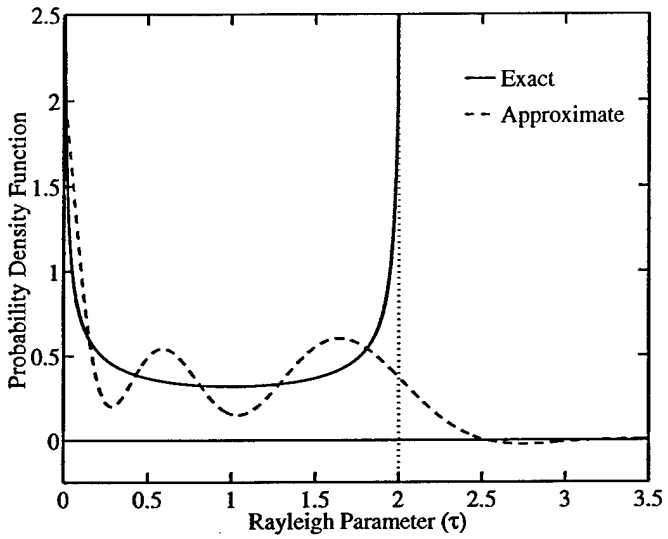

Fig. 2 – The exact and approximate forms of the characteristic PDF for the Nakagami target fluctuation model. The approximation is based on the Padé approximation to the amplitude CF.

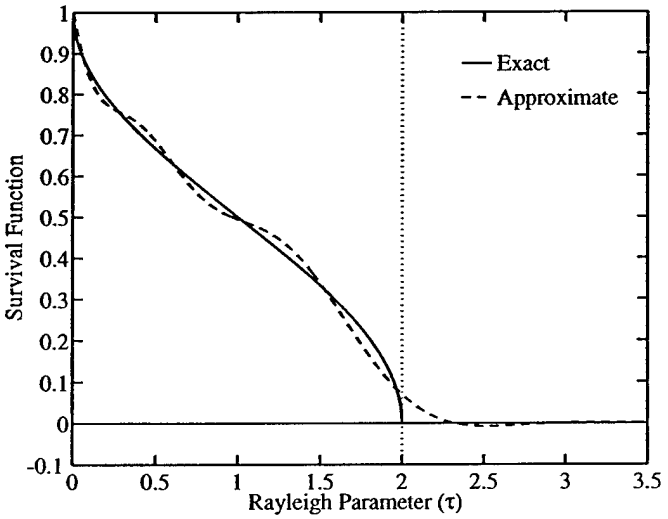

Fig. 3 – The exact and approximate forms of the characteristic SF for the Nakagami target fluctuation model. The approximation is based on the Padé approximation to the amplitude CF.

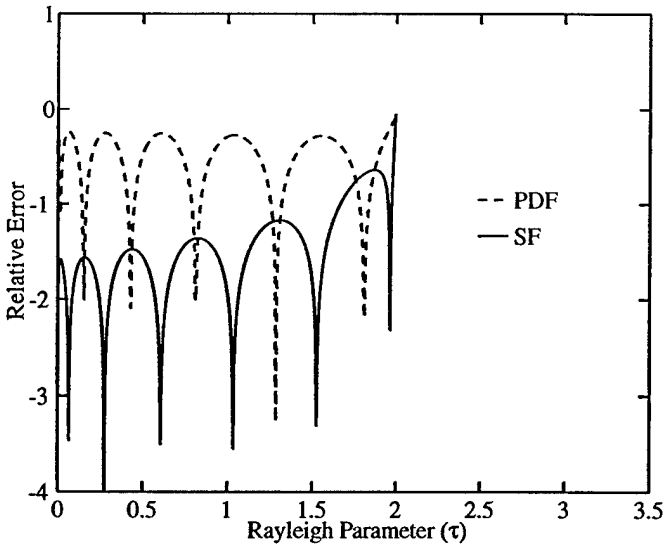

Fig. 4 – The relative errors for the approximations to the characteristic SF and PDF for the Nakagami target fluctuation model that are shown in the previous figures. For $\tau > 2$, the relative error is infinite.

It is well known that the characteristic PDF and SF for this model are given by [14]

$$f_\tau(\tau) = \left(\frac{b^2}{2}\right)^{\nu+1} \frac{\tau^\nu}{\Gamma(\nu+1)} \exp\left(-\frac{b^2\tau}{2}\right) \tag{31}$$

$$S_\tau(\tau) = \frac{\Gamma(\nu+1\,,\, b^2\tau/2)}{\Gamma(\nu+1)}. \tag{32}$$

For $\nu = 0.5$ and $b = \sqrt{3}$, it is shown in Reference 5 that

$$\Phi(\rho) \approx \frac{10.04852}{\rho^2 + 2.932845} - \frac{7.166959}{\rho^2 + 3.403857} - \frac{1.600556}{\rho^2 + 5.813469} - \frac{0.9000533}{\rho^2 + 19.84990}. \tag{33}$$

Substituting the coefficients and poles of the partial fraction expansion in (33) into (16) and (17) and carrying out the algebra yields

$$\begin{aligned} f_\tau(\tau) \approx\ & -0.4500269\exp(-9.924915\tau) - 0.8002768\exp(-2.906733\tau) \\ & -3.583477\exp(-1.7019287\tau) + 5.024257\exp(-1.4664224\tau) \end{aligned} \tag{34}$$

$$\begin{aligned} S_\tau(\tau) \approx\ & -0.04534315\exp(-9.924915\tau) - 0.27531830\exp(-2.906733\tau) \\ & -2.1055389\exp(-1.7019287\tau) + 3.4262004\exp(-1.4664224\tau). \end{aligned} \tag{35}$$

These approximations cannot be visually distinguished from their comparable exact forms in (31) and (32) when displayed on the same graph. Their differences can only be seen from examining the relative error curves shown in Figure 5. They reveal that the approximations generally agree with the exact forms to at least 2 decimal places.

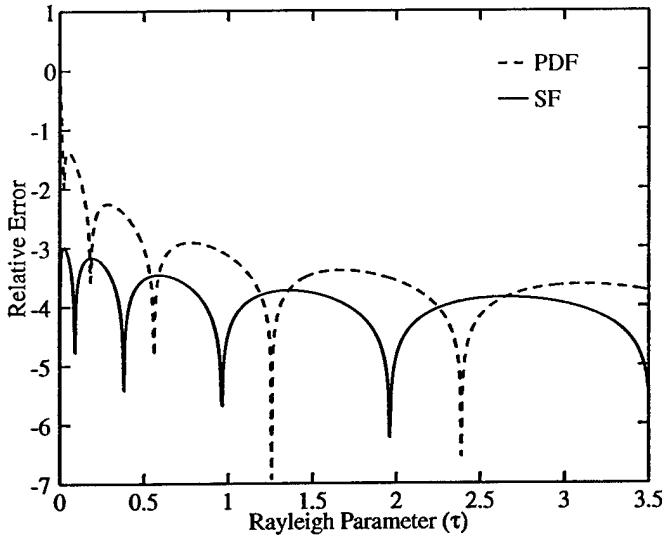

Fig. 5 – The relative errors for the approximations to the characteristic SF and PDF for the K-type clutter fluctuation model.

The Rayleigh Fluctuation Model

As a final example, consider the Rayleigh target and clutter fluctuation model given by

$$f_R(r) = \frac{r}{\sigma^2}\exp\left(-\frac{r^2}{2\sigma^2}\right) \tag{36}$$

$$S_R(r) = \exp\left(-\frac{r^2}{2\sigma^2}\right) \tag{37}$$

$$\Phi(\rho) = \exp\left(-\frac{\sigma^2\rho^2}{2}\right). \tag{38}$$

For $\sigma^2 = 1$ it is easy to see that

$$f_\tau(\tau) = \delta(\tau - \sigma^2) \tag{39}$$

$$S_\tau(\tau) = u_s(\sigma^2 - \tau) \tag{40}$$

where $u_s(\cdot)$ is the unit step function and $\delta(\cdot)$ is its derivative, the Dirac delta function. In Reference 5 it is shown that

$$\begin{aligned}\Phi(\rho) \approx\ & \frac{-204.5260 + j47.68627}{\rho^2 + 10.97484 + j5.196570} + \frac{-204.5260 - j47.68627}{\rho^2 + 10.97484 - j5.196570} \\ & + \frac{58.07762 - j28.55325}{\rho^2 + 8.291362 + j10.38788} + \frac{58.07762 + j28.55325}{\rho^2 + 8.291362 - j10.38788} \\ & + \frac{-4.878310 + j3.723561}{\rho^2 + 2.839304 + j15.61901} + \frac{-4.878310 - j3.723561}{\rho^2 + 2.839304 - j15.61901} \\ & + \frac{302.6534}{\rho^2 + 11.80429}.\end{aligned} \tag{41}$$

Again, substituting the coefficients and poles of the partial fraction expansion in (41) into (16) and (17) and carrying out the algebra yields

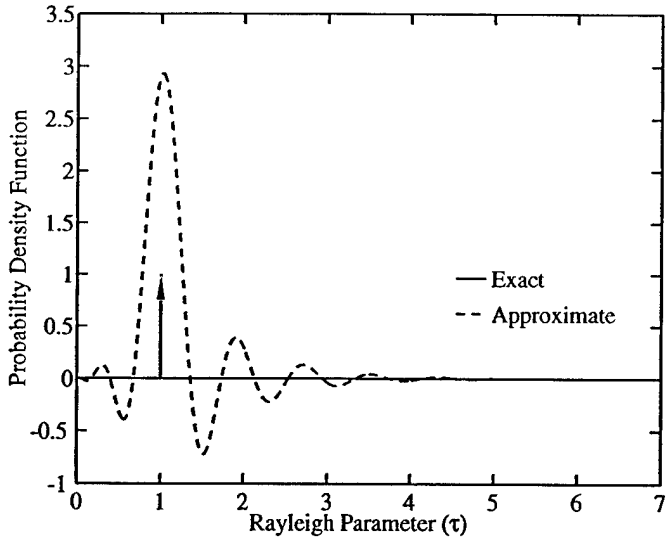

Fig. 6 – The exact and approximate forms of the characteristic PDF for the Rayleigh clutter fluctuation model. The exact form is a Dirac delta function with unity weight. The approximation is based on the Padé approximation to the amplitude CF.

$$\begin{aligned} f_\tau(\tau) \approx\ & 210.0116 \exp(-5.487420\tau) \cos(2.598285\tau - 2.912529803) \\ & +64.71706 \exp(-4.145681\tau) \cos(5.193940\tau + 0.456936839) \\ & +6.137004 \exp(-1.419652\tau) \cos(7.809505\tau - 2.489640610) \\ & +151.3267 \exp(-5.902145\tau) \end{aligned} \tag{42}$$

$$\begin{aligned} S_\tau(\tau) \approx\ & 34.58986 \exp(-5.487420\tau) \cos(2.598285\tau - 2.470307) \\ & +9.738367 \exp(-4.145681\tau) \cos(5.193940\tau + 1.354105) \\ & +0.7731666 \exp(-1.419652\tau) \cos(7.809505\tau - 1.09867) \\ & +25.63927 \exp(-5.902145\tau). \end{aligned} \tag{43}$$

Figures 6 and 7 reveal that (42) and (43) are crude approximations to a delta function and step function. In some intervals they severely violate the properties of the statistical functions they approximate: the PDF approximation can be negative and the SF approximation can be negative or greater than 1. Nevertheless, the amplitude PDF and SF approximations resulting from (41) through (43) are acceptable in that their relative errors are less than -2 for $r < 4.8$ [5].

2.5 Approximate Fluctuation Models Based on Discrete Rayleigh Mixtures

A formula for the characteristic SF, be it exact or approximate, can be used to find approximate discrete Rayleigh mixture formulas for the statistical functions of the Rayleigh parameter and amplitude. In particular, note that

$$S_\tau(\tau) \approx \sum_{k=1}^{N} W_k\, u_s(\tau_k - \tau) \tag{44}$$

and

$$W_k = \int_{(\tau_k+\tau_{k-1})/2}^{(\tau_{k+1}+\tau_k)/2} f_\tau(\tau)\, d\tau = S_\tau\left(\frac{\tau_k + \tau_{k-1}}{2}\right) - S_\tau\left(\frac{\tau_{k+1} + \tau_k}{2}\right) \tag{45}$$

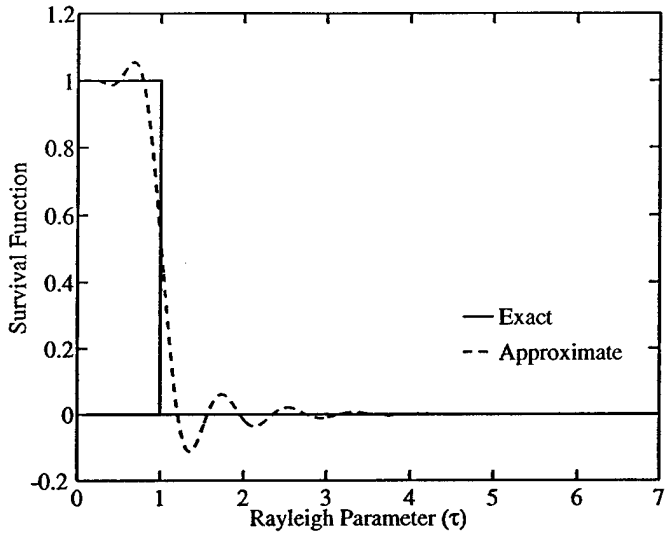

Fig. 7 – The exact and approximate forms of the characteristic SF for the Rayleigh clutter fluctuation model. The exact form is a reversed unit step function. The approximation is based on the Padé approximation to the amplitude CF.

where $\tau_0 = 0$ and the last weight, W_N, is calculated using $\tau_{N+1} = \tau_N + (\tau_N - \tau_{N-1})/2$. It follows that

$$f_\tau(\tau) \approx \sum_{k=1}^{N} W_k \, \delta(\tau - \tau_k) \, . \tag{46}$$

Since the Rayleigh parameter axis can only be sampled at a finite number of points, and because an approximation to the characteristic SF may be used, it was found that to ensure the weights sum to one, any negative weight should be eliminated and the remaining ones should be "normalized" via the mapping

$$W_k \leftarrow \frac{W_k}{W_1 + \ldots + W_N} \, . \tag{47}$$

Substituting (46) into (6) through (8) yields

$$f_R(r) \approx r \sum_{k=1}^{N} \frac{W_k}{\tau_k} \exp\left(-\frac{r^2}{2\tau_k}\right) \tag{48}$$

$$S_R(r) \approx \sum_{k=1}^{N} W_k \exp\left(-\frac{r^2}{2\tau_k}\right) \tag{49}$$

$$\Phi(\rho) \approx \sum_{k=1}^{N} W_k \exp\left(-\frac{\tau_k \rho^2}{2}\right) . \tag{50}$$

Consider the fluctuation models presented in the previous section. For the Nakagami fluctuation model in (19) through (21) with $N = 0.5$ and $\sigma^2 = 1$, inversion of the approximation of the CF in (24) (as a Hankel transform) leads to [5]

$$\begin{aligned} f_R(r) \approx 2 \, \mathrm{Re}\{ & (-19.78778 + \jmath 258.7502) \, r K_0((2.804626 + \jmath 0.2884542) r) \\ & + (30.66573 - \jmath 102.2120) \, r K_0((2.757823 + \jmath 0.8901511) r) \\ & + (-8.790265 + \jmath 9.696267) \, r K_0((2.647426 + \jmath 1.590556) r) \}. \end{aligned} \tag{51}$$

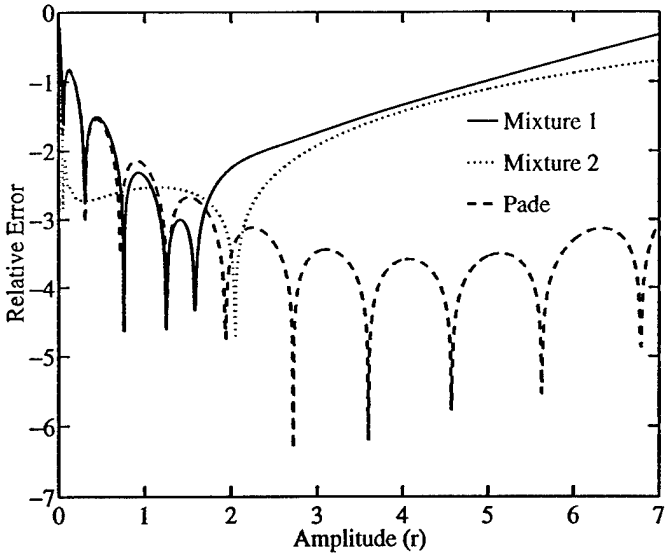

Fig. 8 – The relative error between the exact form of the Nakagami amplitude PDF and a discrete Rayleigh mixture derived from a Padé-based approximation of the characteristic PDF (solid line), a discrete Rayleigh mixture derived from the exact form of the characteristic PDF (dotted line), and the Padé-based approximation to the amplitude PDF (dashed line).

The corresponding approximation to the amplitude SF is

$$\begin{aligned} S_R(r) \approx 2\,\mathrm{Re}\{&(2.407845 + \jmath 92.01074)\, r K_1\left((2.804626 + \jmath 0.2884542)\, r\right) \\ &+ (-0.76368991 - \jmath 36.81605)\, r K_1\left((2.757823 + \jmath 0.8901511)\, r\right) \\ &+ (-0.8228678 + \jmath 4.156900)\, r K_1\left((2.647426 + \jmath 1.590556)\, r\right)\}. \end{aligned} \tag{52}$$

Approximate discrete Rayleigh mixtures to the amplitude PDF and SF were found from the exact forms of the characteristic PDF and SF in (22) and (23), as well as from their Padé-based approximations in (25) and (26). Sampling of the Rayleigh parameter axis was accomplished using the formula

$$\tau_k = \tau_{max}\left(\frac{k\Delta\tau}{\tau_{max}}\right)^{\epsilon} \quad k = 1, \ldots, k_{max}. \tag{53}$$

with $\tau_{max} = 2$, $\Delta\tau = \tau_{max}/k_{max}$, $k_{max} = 30$ and $\epsilon = 3$. This produces a sampling of the Rayleigh parameter axis that is "finer" near $\tau = 0$. This was done to derive accurate discrete Rayleigh mixture approximations to the amplitude PDF and SF near $r = 0$. For this fluctuation model, linear sampling ($\epsilon = 1$) produces less accurate approximations.

Figures 8 and 9 show the relative errors of the amplitude PDF and SF approximations when compared to the closed forms in (19) and (20). Both types of approximation are accurate for $r < 2.5$ where the relative error is generally less than -2.

For the K-type fluctuation model in (28) through (32) with $\nu = 0.5$ and $b = \sqrt{3}$, inversion of the approximation of the CF in (33) (as a Hankel transform) leads to [5]

$$\begin{aligned} f_R(r) \approx\ & 10.04852\, r K_0(1.712555 r) - 7.166959\, r K_0(1.844955 r) \\ & -1.600556\, r K_0(2.411114 r) - 0.9000533\, r K_0(4.455323 r). \end{aligned} \tag{54}$$

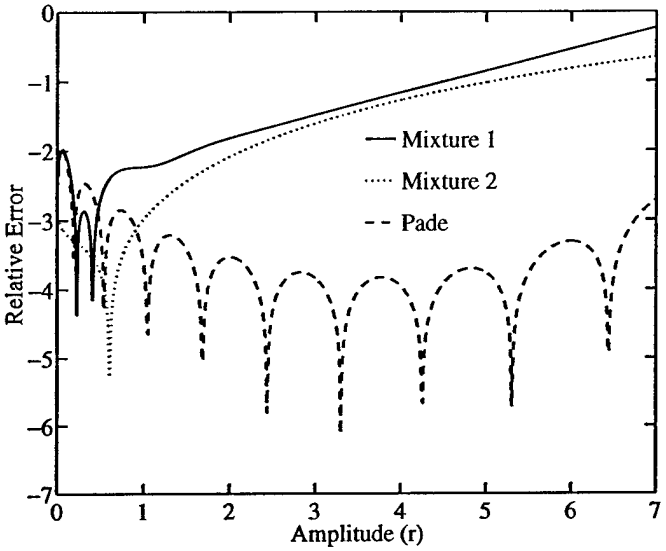

Fig. 9 – The relative error between the exact form of the Nakagami amplitude SF and a discrete Rayleigh mixture derived from a Padé-based approximation of the characteristic SF (solid line), a discrete Rayleigh mixture derived from the exact form of the characteristic SF (dotted line), and the Padé-based approximation to the amplitude SF (dashed line).

The corresponding approximation to the amplitude SF is

$$S_R(r) \approx 5.867560\, rK_1(1.712555r) - 3.884627\, rK_1(1.844955r) \\ -0.6638242\, rK_1(2.411114r) - 0.2020175\, rK_1(4.455323r)\,. \tag{55}$$

Approximate discrete Rayleigh mixtures to the amplitude PDF and SF were found from the exact forms of the characteristic PDF and SF in (31) and (32), as well as from their Padé-based approximations in (34) and (35). Sampling of the Rayleigh parameter axis was accomplished using (53) with $\tau_{max} = 6$, $\Delta\tau = \tau_{max}/k_{max}$, $k_{max} = 30$ and $\epsilon = 2$. Figures 10 and 11 show the relative errors of the PDF and SF approximations when compared to the closed forms in (28) and (29).

Generally the "tails" of the discrete Rayleigh mixture approximations to the PDF and SF are not as accurate as those derived from the Padé approximation to the CF. With proper sampling of the Rayleigh parameter axis, the peaks of the Rayleigh mixture approximations to the amplitude SF are accurate approximations to the true SF and thus provide accurate approximations to useful target detection probabilities, specifically, $0.1 < P_d < 0.9$.

3. MODELING MULTIPLE OBSERVATIONS

3.1 The Observation Vector

Multiple observations of a target can be acquired by processing echoes generated from time-sequential transmissions, frequency sub-bands of a single echo, or a single echo steered to different bearing angles. Suppose that N_d complex matched filter outputs are available and are denoted by

$$y_k = u_k + jv_k \quad \text{for } k = 1, \ldots, N_d\,. \tag{56}$$

These complex numbers can be arranged into a vector of length N_d:

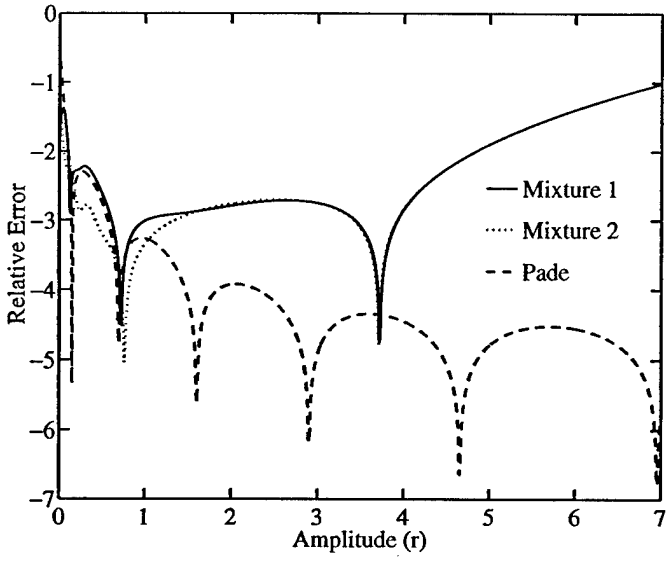

Fig. 10 – The relative error between the exact form of the K-type amplitude PDF and a discrete Rayleigh mixture derived from a Padé-based approximation of the characteristic PDF (solid line), a discrete Rayleigh mixture derived from the exact form of the characteristic PDF (dotted line), and the Padé-based approximation to the amplitude PDF (dashed line).

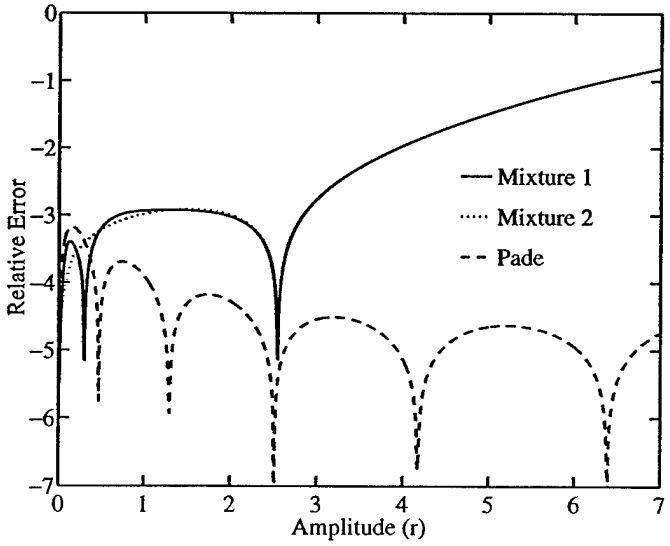

Fig. 11 – The relative error between the exact form of the K-type amplitude SF and a discrete Rayleigh mixture derived from a Padé-based approximation of the characteristic SF (solid line), a discrete Rayleigh mixture derived from the exact form of the characteristic SF (dotted line), and the Padé-based approximation to the amplitude SF (dashed line).

$$\mathbf{y} = \left[\begin{array}{cccc} u_1 + jv_1 & \ldots & u_{N_d} + jv_{N_d} \end{array} \right]^T . \tag{57}$$

Alternately, they may be arranged into a real vector of length $2N_d$:

$$\mathbf{x} = \left[\begin{array}{cccc} u_1 & v_1 & \ldots & u_{N_d} \quad v_{N_d} \end{array} \right]^T . \tag{58}$$

3.2 The Covariance Matrix

In Section 2.1 the assumption of circular symmetry was imposed because of the complete uncertainty in the phase of the complex matched filter output. In the case of multiple observations, the circular symmetry is also imposed for each complex matched filter output, which implies that the real and imaginary parts are zero-mean random variables. This alone is not enough to completely specify the joint PDF, for it is also necessary to assume a certain form of the cross-covariance between the real and imaginary parts of the matched filter outputs.

In an echolocation system, it is reasonable to assume that the correlations between the matched filter outputs do not change if all complex matched filter outputs experience the same phase shift. Consequently, it is shown in Appendix A that for an echolocation system the $2N_d \times 2N_d$ covariance matrix for the real vector $\mathbf{x}$ has the special form

$$E\{\mathbf{x}\mathbf{x}^T\} = \mathbf{R} = [\mathbf{R}_{ik}] \tag{59}$$

where the right side of (59) denotes the matrix as an array of 2×2 sub-matrices of the form

$$\mathbf{R}_{ik} = \left[\begin{array}{cc} E\{u_i u_k\} & E\{u_i v_k\} \\ E\{v_i u_k\} & E\{v_i v_k\} \end{array} \right] = \left\{ \begin{array}{ll} \sigma_k^2 \left[\begin{array}{cc} 1 & 0 \\ 0 & 1 \end{array} \right] & \text{for } i = k \\ \sigma_i \sigma_k \left[\begin{array}{cc} \alpha_{ik} & -\beta_{ik} \\ \beta_{ik} & \alpha_{ik} \end{array} \right] & \text{for } i \neq k \end{array} \right. \tag{60}$$

where α_{ik} and β_{ik} are real numbers. Note that for $i = k$ the sub-matrix is diagonal, which expresses the circular symmetry of the individual complex matched filter outputs. For $i \neq k$, the matrix expresses the additional assumption necessary for echolocation problem: antisymmetric correlation between the real and imaginary parts.

From the sub-matrix in (60) it follows that

$$E\{y_i y_k\} = \left\{ \begin{array}{ll} 2\sigma_k^2 & \text{for } i = k \\ 2\sigma_i \sigma_k (\alpha_{ik} + j\beta_{ik}) & \text{for } i \neq k \end{array} \right. \tag{61}$$

which are the elements of the $N_d \times N_d$ covariance matrix

$$E\{\mathbf{y}\mathbf{y}^H\} = \mathbf{P} \tag{62}$$

where $\mathbf{y}^H$ denotes the Hermitian transpose of the complex vector $\mathbf{y}$.

3.3 The Multidimensional Gaussian Model

It is well known that the multidimensional Gaussian PDF is given by

$$f_{\mathbf{X}}(\mathbf{x}) = \frac{\exp\left(-\frac{1}{2}\mathbf{x}^T\mathbf{R}^{-1}\mathbf{x}\right)}{(2\pi)^{N_d}\sqrt{\det(\mathbf{R})}}. \tag{63}$$

The CF associated with this multidimensional PDF is its $2N_d$-dimensional Fourier transform with respect to the vector of frequency variables

$$\boldsymbol{\mu} = \begin{bmatrix} \omega_1 & \xi_1 & \dots & \omega_{N_d} & \xi_{N_d} \end{bmatrix}^T \tag{64}$$

where ω_k is associated with u_k (real part) and ξ_k is associated with v_k (imaginary part). It is well known that the CF is given by

$$\Phi(\boldsymbol{\mu}) = \exp\left(-\frac{1}{2}\boldsymbol{\mu}^T\mathbf{R}\boldsymbol{\mu}\right). \tag{65}$$

If the matched filter outputs are arranged as a complex random vector whose covariance matrix obeys the properties described in the previous section, then [9,19]

$$f_{\mathbf{Y}}(\mathbf{y}) = \frac{\exp\left(-\mathbf{y}^H\mathbf{P}^{-1}\mathbf{y}\right)}{\pi^{N_d}\det(\mathbf{P})}. \tag{66}$$

Consider the random variable $q = \mathbf{y}^H\mathbf{y}$. Its moment generating function is given by

$$E\left\{\exp\left(t\mathbf{y}^H\mathbf{y}\right)\right\} = E\left\{\exp\left(tq\right)\right\} \tag{67}$$

It is straightforward to show that [17,19]

$$E\left\{\exp\left(t\mathbf{y}^H\mathbf{y}\right)\right\} = \frac{1}{\det(\mathbf{I}-t\mathbf{P})} = \prod_{i=1}^{N_d}\frac{1}{1-t\lambda_i} = \sum_{i=1}^{N_d}\frac{D_i}{(1-t\lambda_i)^{n_i}} \tag{68}$$

where $\lambda_1 \dots \lambda_{N_d}$ are the eigenvalues of the covariance matrix $\mathbf{P}$ and the last equality is the result of a partial fraction expansion with parameters D_i and n_i. Inverting this function (as a Laplace transform) yields the PDF of q to be

$$f_Q(q) \approx \sum_{i=1}^{N_d}\frac{D_i}{\lambda_i^{n_i}\Gamma(n_i)}q^{n_i-1}\exp\left(-\frac{q}{\lambda_i}\right). \tag{69}$$

The amplitude of the vector $\mathbf{y}$ is $w = \sqrt{q}$, so by a transformation of random variable, it follows that

$$f_W(w) \approx \sum_{i=1}^{N_d}\frac{2D_i}{\lambda_i^{n_i}\Gamma(n_i)}w^{2n_i-1}\exp\left(-\frac{w^2}{\lambda_i}\right). \tag{70}$$

Integration of (70) yields

$$S_W(w) \approx \sum_{i=1}^{N_d}\frac{D_i}{\Gamma(n_i)}\Gamma\left(n_i, \frac{w^2}{\lambda_i}\right). \tag{71}$$

If $n_i = 1$ for all i (which is typically the case), then (71) reduces to

$$S_W(w) \approx \sum_{i=1}^{N_d} D_i \exp\left(-\frac{w^2}{\lambda_i}\right). \tag{72}$$

3.4 The Spherically Invariant Random Vector Model

A generalization of a random process that follows the Rayleigh mixture fluctuation model in Section 2.2 is the *spherically invariant random process* (SIRP) that produces *spherically invariant random vectors* (SIRVs) [1,2,3,8,13-15,19,20]. The PDFs for SIRVs are a generalization of (6) and are given by

$$f_{\mathbf{X}}(\mathbf{x}) = \frac{1}{(2\pi)^{N_d}\sqrt{\det(\mathbf{R})}} \int_0^\infty \frac{1}{\tau^{N_d}} \exp\left(-\frac{1}{2\tau}\mathbf{x}^T\mathbf{R}^{-1}\mathbf{x}\right) f_\tau(\tau)\, d\tau \tag{73}$$

$$f_{\mathbf{Y}}(\mathbf{y}) = \frac{1}{\pi^{N_d}\det(\mathbf{P})} \int_0^\infty \frac{1}{\tau^{N_d}} \exp\left(-\frac{1}{\tau}\mathbf{y}^H\mathbf{P}^{-1}\mathbf{y}\right) f_\tau(\tau)\, d\tau. \tag{74}$$

The CF for a SIRV is a generalization of (8) given by

$$\Phi(\boldsymbol{\mu}) = \Phi\left(\boldsymbol{\mu}^T\mathbf{R}\boldsymbol{\mu}\right) = \int_0^\infty \exp\left(-\frac{\tau}{2}\boldsymbol{\mu}^T\mathbf{R}\boldsymbol{\mu}\right) f_\tau(\tau)\, d\tau. \tag{75}$$

It can be show that the PDF for a SIRV has an alternate representation that is a generalization of the Hankel transform. In Reference 13 it is shown that

$$f_{\mathbf{X}}(\mathbf{x}) = \frac{h\left(\mathbf{x}^T\mathbf{R}^{-1}\mathbf{x}\right)}{(2\pi)^{N_d}\sqrt{\det(\mathbf{R})}} \tag{76}$$

$$f_{\mathbf{Y}}(\mathbf{y}) = \frac{h\left(2\mathbf{y}^H\mathbf{P}^{-1}\mathbf{y}\right)}{\pi^{N_d}\det(\mathbf{P})} \tag{77}$$

where $h(\cdot)$ characterizes the square magnitude of the vector $\mathbf{y}$ and is given by

$$h(\zeta) = \frac{1}{\left(\sqrt{\zeta}\right)^{N_d-1}} \int_0^\infty \rho^{N_d}\Phi(\rho)J_{N_d-1}\left(\sqrt{\zeta}\rho\right)\, d\rho. \tag{78}$$

Note that (77) is a generalization of the multidimensional Gaussian PDF and reduces to this PDF when $h(\zeta) = \exp(-\zeta/2)$. Furthermore, (76) and (77) show that $\sqrt{\mathbf{y}^H\mathbf{P}^{-1}\mathbf{y}} = \sqrt{\mathbf{x}^T\mathbf{R}^{-1}\mathbf{x}/2}$ [9].

3.5 Approximate Amplitude Fluctuation Models Based on Padé Approximations

The approximations to the PDF, SF and CF for single observations that are based on Padé approximations to the CF (presented in Section 2.3) can be immediately generalized to the case of multiple observations. From (78) it can be seen that $h(\cdot)$ is only dependent upon the circularly symmetric CF, which is given by (75) and is approximated by

$$\Phi(\boldsymbol{\mu}) \approx \sum_{k=1}^{M} \frac{A_k}{\left[\boldsymbol{\mu}^T\mathbf{R}\boldsymbol{\mu}/(2\eta) - p_k\right]^{m_k}} \tag{79}$$

where division of the argument by 2η maintains the expected power of each element of $\mathbf{x}$ as given by the matrix $\mathbf{R}$. It should be noted that η is not a free parameter but is given by

$$\eta = \sum_{k=1}^{M} \frac{m_k A_k}{(-p_k)^{m_k+1}} \tag{80}$$

and constrains the second radial moment to be $E\{\mathbf{x}^T\mathbf{R}^{-1}\mathbf{x}\} = 2N_d$. It is shown in Appendix B that η is proportional to the expected power of the matched filter output for a single observation. Formal inversion of (79) (as a Hankel transform) using Eq. (2) on page 434 of Reference 18 yields

$$h(\zeta) \approx (2\eta)^{N_d} \sum_{k=1}^{M} \frac{A_k(-p_k)^{N_d-m_k}}{2^{m_k-1}\Gamma(m_k)} \frac{K_{N_d-m_k}\left(\sqrt{-2\eta p_k \zeta}\right)}{\left(\sqrt{-2\eta p_k \zeta}\right)^{N_d-m_k}}. \tag{81}$$

It follows from (77) that

$$f_{\mathbf{Y}}(\mathbf{y}) \approx \frac{(2\eta)^{N_d}}{\pi^{N_d}\det(\mathbf{P})} \sum_{k=1}^{M} \frac{A_k(-p_k)^{N_d-m_k}}{2^{m_k-1}\Gamma(m_k)} \frac{K_{N_d-m_k}\left(\sqrt{-4\eta p_k \mathbf{y}^H\mathbf{P}^{-1}\mathbf{y}}\right)}{\left(\sqrt{-4\eta p_k \mathbf{y}^H\mathbf{P}^{-1}\mathbf{y}}\right)^{N_d-m_k}}. \tag{82}$$

An alternate way to arrive at (82) is to substitute the Padé-based approximation to the characteristic PDF in (16) into (74) and carry out the integration using Eq. (15) on page 183 of Reference 18. This avoids an apparent problem with the Hankel transform inversion of (79): the inversion integral as given by Eq. (2) on page 434 of Reference 18 is valid only when $0 < N_d < 2m_k - 3/2$, a restriction that is easily violated in practice[4].

Invoking the multidimensional transformation of random variable $r = \sqrt{\mathbf{y}^H\mathbf{P}^{-1}\mathbf{y}}$ yields [13]

$$f_R(r) \approx \frac{4}{\Gamma(N_d)} \sum_{k=1}^{M} \frac{A_k(-p_k)^{(N_d-m_k)/2}\eta^{(N_d+m_k)/2}}{\Gamma(m_k)} r^{N_d+m_k-1} K_{N_d-m_k}\left(\sqrt{-4\eta p_k}\, r\right). \tag{83}$$

Closed-form integration of (83) is only possible when $m_k = 1$ (which is usually the case) or $N_d = 1$, thus

$$S_R(r) \approx \frac{2\eta^{N_d/2}}{\Gamma(N_d)} \sum_{k=1}^{M} A_k(-p_k)^{N_d/2-1} r^{N_d} K_{N_d}\left(\sqrt{-4\eta p_k}\, r\right). \tag{84}$$

For $m_k > 1$, approximations to the integral of $r^{N_d+m_k-1}K_{N_d-m_k}\left(\sqrt{-4\eta p_k}\, r\right)$ must be used, some of which may be found in Reference 11. For example, by using the large-argument asymptotic form

$$K_\nu(t) \approx \sqrt{\frac{\pi}{2t}}\exp(-t) \tag{85}$$

in (83) and integrating, it follows that

$$S_R(r) \approx \frac{\sqrt{8\pi}}{2^{N_d}\Gamma(N_d)} \sum_{k=1}^{M} \frac{A_k}{2^{m_k}\Gamma(m_k)(-p_k)^{m_k}} \Gamma\left(N_d + m_k - 1/2\,,\sqrt{-4\eta p_k}\, r\right). \tag{86}$$

It is demonstrated in Reference 5 that the Padé-based approximations are generally suitable for approximating the tails of the PDF and SF in single-observation detection problems. This allows accurate calculation of false alarm probabilities, which are typically less than 0.001. It is expected that this is also true for multiple-observation detection problems.

[4] We are reporting the work of earlier researchers in this field who ignored this restriction.

3.6 Approximate Fluctuation Models Based on Discrete Rayleigh Mixtures

Generalization of the discrete Rayleigh mixture statistical functions in Section 2.5 is also immediate. Thus, it follows that if the characteristic PDF is given by (46), then discrete Rayleigh mixture approximations to (73), (74) and (75) are

$$f_{\mathbf{X}}(\mathbf{x}) \approx \frac{1}{(2\pi)^{N_d}} \sum_{l=1}^{N} W_k \frac{\exp\left[-\frac{1}{2}\mathbf{x}^T(\tau_k\mathbf{R})^{-1}\mathbf{x}\right]}{\sqrt{\det(\tau_k\mathbf{R})}} \tag{87}$$

$$f_{\mathbf{Y}}(\mathbf{y}) \approx \frac{1}{\pi^{N_d}} \sum_{l=1}^{N} W_k \frac{\exp\left[-\mathbf{y}^H(\tau_k\mathbf{P})^{-1}\mathbf{y}\right]}{\det(\tau_k\mathbf{P})} \tag{88}$$

$$\Phi(\boldsymbol{\mu}) \approx \sum_{k=1}^{N} W_k \exp\left(-\frac{\tau_k}{2}\boldsymbol{\mu}^T\mathbf{R}\boldsymbol{\mu}\right). \tag{89}$$

Since the individual terms composing (87) and (88) are Gaussian PDFs, the PDF and SF of the amplitude $w = \sqrt{\mathbf{y}^H\mathbf{y}} = \sqrt{\mathbf{x}^T\mathbf{x}}$ are simply mixtures based on (70) and (71). Thus,

$$f_W(w) \approx \sum_{k=1}^{N} W_k \left[\sum_{i=1}^{N_d} \frac{2D_i}{(\tau_k\lambda_i)^{n_i}\Gamma(n_i)} w^{2n_i-1} \exp\left(-\frac{w^2}{\tau_k\lambda_i}\right)\right] \tag{90}$$

$$S_W(w) \approx \sum_{k=1}^{N} W_k \left[\sum_{i=1}^{N_d} \frac{D_i}{\Gamma(n_i)} \Gamma\left(n_i, \frac{w^2}{\tau_k\lambda_i}\right)\right]. \tag{91}$$

where λ_i, n_i and D_i are as defined in (68). If $n_i = 1$ for all i (which is typically the case), then (91) reduces to

$$S_W(w) \approx \sum_{k=1}^{N} W_k \left[\sum_{i=1}^{N_d} D_i \exp\left(-\frac{w^2}{\tau_k\lambda_i}\right)\right]. \tag{92}$$

3.7 The Receiver Structure

The receiver structure for multiple observations is shown in Figure 12 and is a generalization of the normalized matched filter employed for processing a single echo. The normalization is accomplished by the multiplication of the observation vector, $\mathbf{y}$, by the inverse square root of the clutter covariance matrix, $\mathbf{P_C}$, where $\mathbf{P_C} = \mathbf{P_C^{1/2}}\mathbf{P_C^{1/2}}$. The resulting normalized observation vector, $\mathbf{z}$, whose covariance matrix is the identity matrix when the input is only clutter, is followed by an envelope detector. If the detection statistic ,r, exceeds the threshold, γ, a target is declared present (hypothesis H_1), otherwise, only clutter is assumed to be present (hypothesis H_0).

If the clutter and target fluctuation models follow any of the classic Swerling models, then the receiver structure shown in Figure 1 is "optimal" in the sense that it maximizes a likelihood function [4]. The receiver structure is not optimal in any sense for detecting targets in non-Gaussian clutter. It is addressed here because it is a simple, well understood structure that is easy to implement. Furthermore, unlike receivers based on the likelihood ratio, it is not dependent upon the statistical nature of the target or clutter.

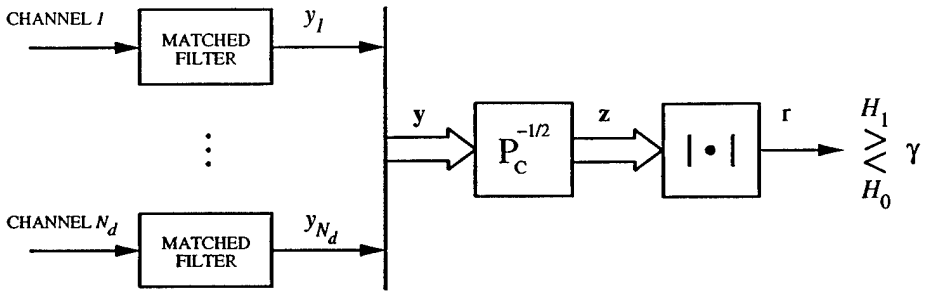

Fig. 12 – The multi-dimensional normalized matched filter receiver structure.

3.8 Setting the Detection Threshold

The detection threshold, γ, is set by solving the non-linear equation

$$S_R(\gamma) - P_{fa} = 0 \tag{93}$$

where $S_R(r)$ is either an exact or approximate form. Using Newton's method results in the following recursive equation that usually converges to the solution of (93):

$$\gamma_{k+1} = \gamma_k + \frac{P_{fa} - S_R(\gamma_k)}{f_R(\gamma_k)} \tag{94}$$

where γ_0 is an initial value (guess) of the threshold.

3.9 Calculating the Probability of Detection

The Rayleigh mixture approximations can be used to calculate detection probabilities. Consider the following approximations to the CFs for the target and clutter amplitude fluctuation models:

$$\Phi(\boldsymbol{\mu}|\text{target}) \approx \sum_{k=1}^{N_T} W_{T,k} \exp\left(-\frac{\tau_{T,k}}{2}\boldsymbol{\mu}^T \mathbf{R}_T \boldsymbol{\mu}\right) \tag{95}$$

$$\Phi(\boldsymbol{\mu}|\text{clutter}) \approx \sum_{l=1}^{N_C} W_{C,l} \exp\left(-\frac{\tau_{C,l}}{2}\boldsymbol{\mu}^T \mathbf{R}_C \boldsymbol{\mu}\right). \tag{96}$$

Since the CFs are multidimensional Fourier transforms of the PDFs, the CF for the target-plus-clutter case can be found by multiplying the CFs:

$$\begin{aligned}\Phi(\boldsymbol{\mu}|H_1) &= \Phi(\boldsymbol{\mu}|\text{target})\Phi(\boldsymbol{\mu}|\text{clutter}) \\ &\approx \sum_{k=1,l=1}^{N_T,N_C} W_{T,k}\, W_{C,l} \exp\left[-\frac{1}{2}\boldsymbol{\mu}^T\left(\tau_{T,k}\mathbf{R}_T + \tau_{C,l}\mathbf{R}_C\right)\boldsymbol{\mu}\right].\end{aligned} \tag{97}$$

Since the term in the summation above are merely the CFs associated with multidimensional Gaussian PDFs, from (63) through (66) it follows that the PDFs associated with this CF are

$$f_{\mathbf{X}}(\mathbf{x}|H_1) \approx \frac{1}{(2\pi)^{N_d}} \sum_{k=1,l=1}^{N_T,N_C} W_{T,k}\, W_{C,l} \frac{\exp\left[-\frac{1}{2}\mathbf{x}^T \left(\tau_{T,k}\mathbf{R}_T + \tau_{C,l}\mathbf{R}_C\right)^{-1}\mathbf{x}\right]}{\sqrt{\det(\tau_{T,k}\mathbf{R}_T + \tau_{C,l}\mathbf{R}_C)}} \tag{98}$$

$$f_{\mathbf{Y}}(\mathbf{y}|H_1) \approx \frac{1}{\pi^{N_d}} \sum_{k=1,l=1}^{N_T,N_C} W_{T,k}\, W_{C,l} \frac{\exp\left[-\mathbf{y}^H \left(\tau_{T,k}\mathbf{P}_T + \tau_{C,l}\mathbf{P}_C\right)^{-1}\mathbf{y}\right]}{\det(\tau_{T,k}\mathbf{P}_T + \tau_{C,l}\mathbf{P}_C)}. \tag{99}$$

Detection is performed on the magnitude of the normalized multi-dimensional output, $\mathbf{z} = \mathbf{P}_C^{-1/2}\mathbf{y}$. Thus, by this transformation of random variable, the PDF of $\mathbf{z}$ is

$$f_{\mathbf{Z}}(\mathbf{z}|H_1) \approx \frac{1}{\pi^{N_d}} \sum_{k=1,l=1}^{N_T,N_C} W_{T,k}\, W_{C,l} \frac{\exp\left[-\mathbf{z}^H \left(\tau_{C,l}\mathbf{I} + \tau_{T,k}\mathbf{P}_C^{-1/2}\mathbf{P}_T\mathbf{P}_C^{-1/2}\right)^{-1}\mathbf{z}\right]}{\det\left(\tau_{C,l}\mathbf{I} + \tau_{T,k}\mathbf{P}_C^{-1/2}\mathbf{P}_T\mathbf{P}_C^{-1/2}\right)}. \tag{100}$$

The PDF of $r = \sqrt{\mathbf{y}^H\mathbf{P}^{-1}\mathbf{y}} = \sqrt{\mathbf{z}^H\mathbf{z}} = w$ follows from (70) and is

$$f_R(r|H_1) \approx \sum_{k=1,l=1}^{N_T,N_C} W_{T,k}\, W_{C,l} \left[\sum_{i=1}^{N_d} \frac{2D_{i,k,l}}{\lambda_{i,k,l}^{n_{i,k,l}}\Gamma\left(n_{i,k,l}\right)} r^{2n_{i,k,l}-1} \exp\left(-\frac{r^2}{\lambda_{i,k,l}}\right)\right] \tag{101}$$

where $\lambda_{1,k,l} \ldots \lambda_{N_d,k,l}$ are the eigenvalues of the covariance matrix $\tau_{C,l}\mathbf{I} + \tau_{T,k}\mathbf{P}_C^{-1/2}\mathbf{P}_T\mathbf{P}_C^{-1/2}$ and $n_{1,k,l} \ldots, n_{N_d,k,l}$ denote their respective powers in the partial fraction expansion. Integration of (101) leads to

$$S_R(r|H_1) \approx \sum_{k=1,l=1}^{N_T,N_C} W_{T,k}\, W_{C,l} \left[\sum_{i=1}^{N_d} \frac{D_{i,k,l}}{\Gamma\left(n_{i,k,l}\right)} \Gamma\left(n_{i,k,l}\,, \frac{r^2}{\lambda_{i,k,l}}\right)\right]. \tag{102}$$

If $n_{i,k,l} = 1$ (which is usually the case), then (102) simplified to

$$S_R(r|H_1) \approx \sum_{k=1,l=1}^{N_T,N_C} W_{T,k}\, W_{C,l} \left[\sum_{i=1}^{N_d} D_{i,k,l} \exp\left(-\frac{r^2}{\lambda_{i,k,l}}\right)\right]. \tag{103}$$

The SFs in (102) and (103) provide the detection probabilities when evaluated at the detection threshold ($r = \gamma$).

3.10 Examples

The Accuracy of Target-Plus-Clutter Models

The example in this section quantifies the possible accuracy of using Rayleigh mixture approximations to calculate the statistical functions of a non-Rayleigh target in non-Rayleigh clutter for multiple observations. A case is examined where the individual multidimensional statistical functions are known in closed form but the PDF for the sum of random vectors is not. In general the statistical functions of the target-plus-clutter case cannot be found in closed form. However, it is possible to compare the one-dimensional (complex) projection of the joint PDF with their corresponding exact analytic forms in special cases.

Consider the case of four complex matched filter outputs ($N_d = 4$) for a K-type target[5] ($\mathbf{y}_1$) in K-type clutter ($\mathbf{y}_2$), each with joint PDFs between their real and imaginary parts given by

[5]Because the resulting target-plus-clutter amplitude PDF and SF can be expressed in closed form (shown later), this choice of target model is only a mathematical convenience.

$$f_{\mathbf{x}_i}(\mathbf{x}) = \frac{b_i^8}{3(4\pi)^4 \det(\mathbf{M}_i)} K_0\left(b_i\sqrt{\mathbf{y}^H \mathbf{M}_i^{-1}\mathbf{y}}\right) \quad \text{for } i = 1,2 \tag{104}$$

where $b_1 = 0.5$, $b_2 = 0.75$ and

$$\mathbf{M}_1 = \begin{bmatrix} 0.7092 & 0.5390 + 0.0385\jmath & 0.4749 - 0.0186\jmath & 0.5392 + 0.0669\jmath \\ 0.5390 - 0.0385\jmath & 0.6577 & 0.4587 - 0.0437\jmath & 0.5092 + 0.0090\jmath \\ 0.4749 + 0.0186\jmath & 0.4587 + 0.0437\jmath & 0.6170 & 0.4891 + 0.0391\jmath \\ 0.5392 - 0.0669\jmath & 0.5092 - 0.0090\jmath & 0.4891 - 0.0391\jmath & 0.6930 \end{bmatrix} \tag{105}$$

$$\mathbf{M}_2 = \begin{bmatrix} 0.6532 & 0.4995 - 0.0519\jmath & 0.4764 + 0.0127\jmath & 0.4971 - 0.0426\jmath \\ 0.4995 + 0.0519\jmath & 0.6559 & 0.4902 + 0.0463\jmath & 0.5167 - 0.0137\jmath \\ 0.4764 - 0.0127\jmath & 0.4902 - 0.0463\jmath & 0.6168 & 0.4815 - 0.0378\jmath \\ 0.4971 + 0.0426\jmath & 0.5167 + 0.0137\jmath & 0.4815 + 0.0378\jmath & 0.6701 \end{bmatrix}. \tag{106}$$

The characteristic functions of these models are

$$\Phi(\rho) = \frac{1}{1 + (\rho/b_i)^2}, \quad \text{for } i = 1,2. \tag{107}$$

The CF for the new random variable $\mathbf{y} = \mathbf{y}_1 + \mathbf{y}_2$ is the product of the CFs in (107) whose partial fraction expansion is

$$\Phi(\rho) = \frac{b_1^2 b_2^2}{b_2^2 - b_1^2}\left[\frac{1}{1 + (\rho/b_1)^2} - \frac{1}{1 + (\rho/b_2)^2}\right] \tag{108}$$

which can be inverted (as a Hankel transform) to yield the one-dimensional amplitude PDF and SF as

$$f_R(r) = \frac{b_1^2 b_2^2}{b_2^2 - b_1^2} r\,[K_0(b_1 r) - K_0(b_2 r)] \tag{109}$$

$$S_R(r) = \frac{b_1^2 b_2^2}{b_2^2 - b_1^2} r\left[\frac{1}{b_1}K_1(b_1 r) - \frac{1}{b_2}K_1(b_2 r)\right]. \tag{110}$$

As noted above, the closed-form expressions for the PDF and SF of $\mathbf{x}$ cannot be found, but the projection of the random variables given by

$$r = \sqrt{\mathbf{x}^T A \mathbf{x}} \tag{111}$$

where

$$\mathbf{A} = \text{Diag}[1,0,0,0] \tag{112}$$

or any other permutation of the elements of A, follow the statistical functions in (109) and (110).

Rayleigh mixture approximations to (109) and (110) were calculated using the procedure in Section 3.9 using the sampling of the Rayleigh parameter axis given by (53) with $\tau_{max} = 15/b_i^2$, $k_{max} = 50$, $\Delta\tau = \tau_{max}/k_{max}$, and $\epsilon = 2$. The relative errors of the Rayleigh mixtures are shown in Figure 13. Except for a small interval near $r = 0$, these approximations show good agreement with the closed form expressions.

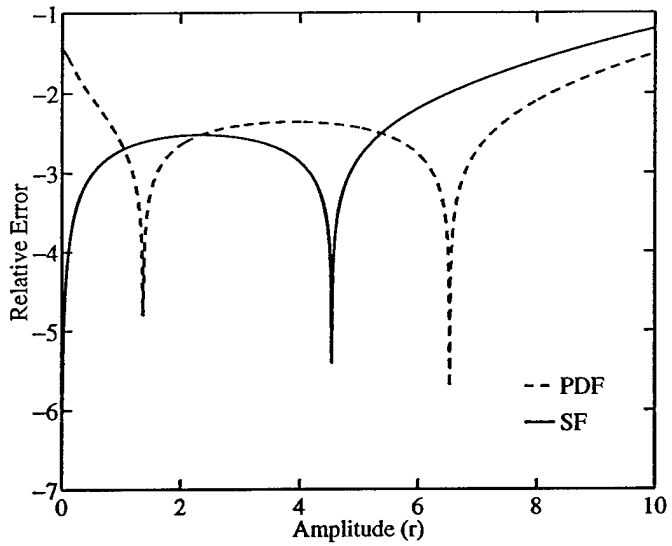

Fig. 13 – The relative errors between the closed form SF and PDF of the projection and their Rayleigh mixture approximations.

Calculations of ROC curves

Consider the case of a Nakagami fluctuating target in clutter following a K-type fluctuation model. The parameters of these models are the same as those presented in Section 2.4. Let $N_d = 4$ with the elements of the complex covariance matrix $\mathbf{P_T}$ following the Markov form

$$E\{y_i y_k\} = 0.8 \exp\left(-\frac{j\pi|i-k|}{3}\right). \tag{113}$$

Let the complex covariance matrix $\mathbf{P_C}$ be the identity matrix, thus modeling the case of uncorrelated clutter. Finally, let the SCR be defined by

$$\text{SCR} = \frac{\text{trace}(\mathbf{P_T})}{\text{trace}(\mathbf{P_C})} \tag{114}$$

which is the total target echo power (from all matched filter outputs) divided by the total clutter power.

The receiver operating characteristic (ROC) curves were calculated for this combination of fluctuation models using the procedure outlined Sections 3.8 and 3.9. Padé-based approximations to the SF (described in Section 3.5) were used to calculate the detection threshold. Discrete Rayleigh mixture models (described in Section 3.6) were used to calculate P_d. In particular, the exact form of the characteristic SF for the Nakagami model was used to calculate its approximate discrete Rayleigh mixture model, whereas the Padé-based SF approximation was used for the K-type approximate mixture model.

The ROC curves plotted on total probability scales are shown in Figures 14 through 16, each showing P_d for a different P_{fa}. Four ROC curves are shown in each figure: Rayleigh target in Rayleigh clutter, $N_d = 1$ (dotted line); Nakagami target in K-type clutter, $N_d = 4$, uncorrelated target (dashed line); Nakagami target in K-type clutter, $N_d = 4$, correlated target (solid line); Nakagami target in K-type clutter, $N_d = 1$ (dot-dash line).

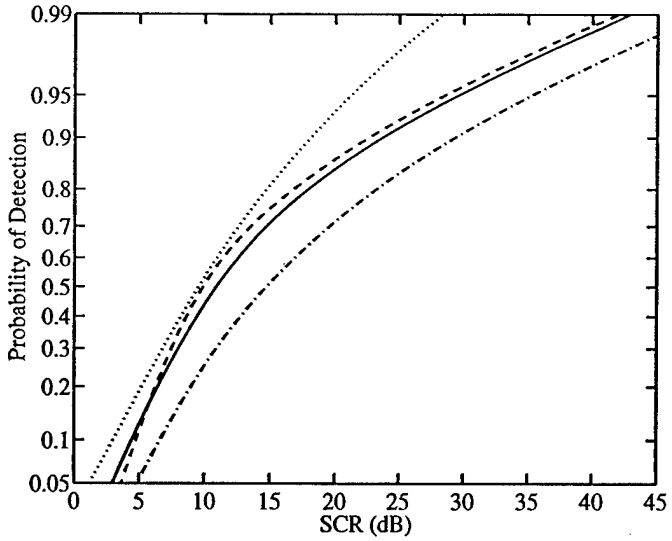

Fig. 14 – The ROC curves for $P_{fa} = 0.001$: Rayleigh target in Rayleigh clutter, $N_d = 1$ (dotted line); Nakagami target in K-type clutter, $N_d = 4$, uncorrelated target (dashed line); Nakagami target in K-type clutter, $N_d = 4$, correlated target (solid line); Nakagami target in K-type clutter, $N_d = 1$ (dot-dash line).

As expected, using multiple observations yields higher detection probabilities. The curves for the uncorrelated target are nearly identical in shape to the ROC curve for correlated target observations, but are shifted approximately 1 dB to the left. The ROC curves for the Rayleigh target in Rayleigh clutter are well known and obey the equation

$$P_d = P_{fa}^{1/(1+\mathrm{SCR})}. \tag{115}$$

They have been included for reference since they may be regarded as standard set of ROC curves. Clearly the mathematical form of the fluctuation models have a profound effect on the performance of a detection system.

It was found that when using total probability scales to plot ROC curves, as was done in Figures 14 through 16, small variations in the curves arising from the use of different approximations will be exaggerated for $P_d > 0.9$. This should not be of great concern because it is the portion of a ROC curve where $0.1 < P_d < 0.9$ that is the most useful.

4. CONCLUSIONS

The mathematical techniques presented in this report allow accurate computation of detection probabilities over a range of values considered critical in the performance evaluation of echolocation systems. The Padé-based approximations, which generally provide good approximations to PDF tails, are suitable for calculating detection thresholds. The approximations based on discrete Rayleigh mixtures provide good approximations to PDF modes (peaks) that generally affect the probability of detection.

Though the techniques presented here appear complicated, especially in light of the matrix calculations that must be performed, it was found that implementation was straightforward using *Matlab*.

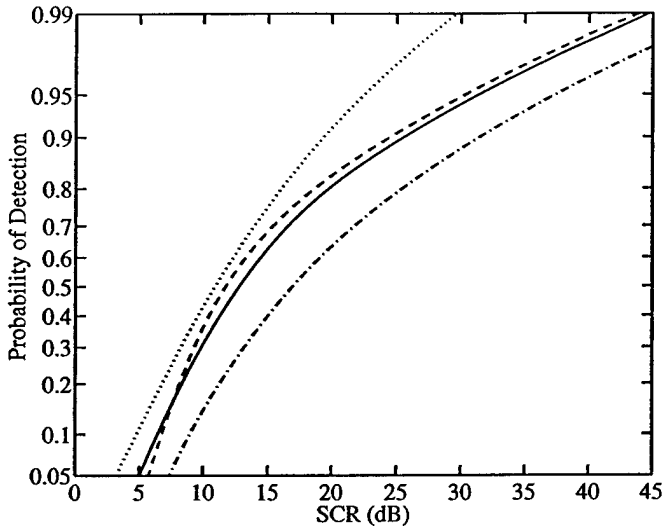

Fig. 15 – The ROC curves for $P_{fa} = 0.0001$: Rayleigh target in Rayleigh clutter, $N_d = 1$ (dotted line); Nakagami target in K-type clutter, $N_d = 4$, uncorrelated target (dashed line); Nakagami target in K-type clutter, $N_d = 4$, correlated target (solid line); Nakagami target in K-type clutter, $N_d = 1$ (dot-dash line).

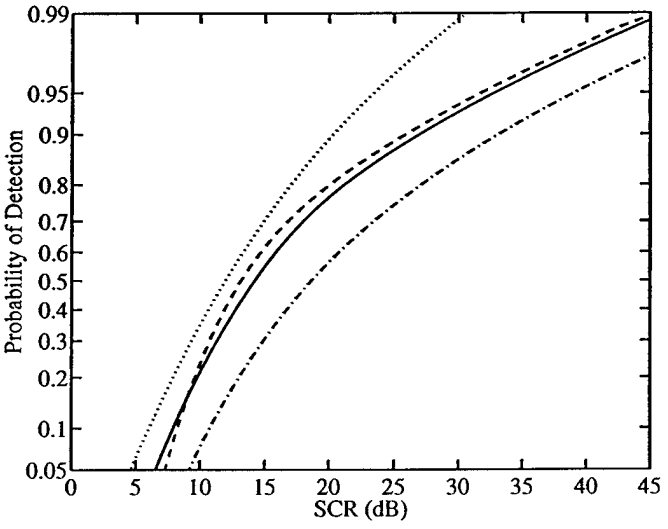

Fig. 16 – The ROC curves for $P_{fa} = 0.00001$: Rayleigh target in Rayleigh clutter, $N_d = 1$ (dotted line); Nakagami target in K-type clutter, $N_d = 4$, uncorrelated target (dashed line); Nakagami target in K-type clutter, $N_d = 4$, correlated target (solid line); Nakagami target in K-type clutter, $N_d = 1$ (dot-dash line).

Implementation of the techniques presented here requires some human intervention. For example, choosing the order of the Padé approximations, the sampling of the characteristic SF and assessing the quality of the resulting statistical function approximations requires some judgment by an analyst. Consequently, the techniques presented herein are best suited for off-line performance prediction.

5. ACKNOWLEDGMENTS

The authors are grateful to Dr. Sudha Reese and Mr. Roger Pridham of the Raytheon Corporation for suggesting that the Padé-based approximation techniques for characterizing single-observation detection systems could be extended to the case of multiple observations. The authors are also grateful to Ms. Nancy Harned of the Office of Naval Research, Code 321US for funding the preparation and publication of this report.

The authors may be contacted at the follow e-mail addresses: *drumheller@nrl.navy.mil* and *henry.lew@dsto.defence.gov.au*.

6. REFERENCES

1. Blake, I. F., "On a class of processes arising in linear estimation theory," *IEEE Transactions on Information Theory*, Vol. IT-14, No. 1, 12-16 (1968).
2. Conte, E., and Longo, M., "Characterization of radar clutter as a spherically invariant random process," *IEE Proceedings*, Vol. 134, Pt. F, No. 2, 191-197 (1987).
3. Conte, E., DiBisceglie, M., Longo, M., and Lops, M., "Canonical detection in spherically invariance noise," *IEEE Transactions on Communications*, Vol. 43, No. 2/3/4, 416-424 (1995).
4. DiFranco, J. V. and Rubin, W. L. , *Radar Detection*, Artech House, Inc., Dedham, MA, 1980.
5. Drumheller, D. M., "Padé approximations to matched filter amplitude probability functions," *IEEE Transactions on Aerospace and Electronic Systems*, AES-35, No. 3 (1999).
6. Drumheller, D. M. and Lew, H. "Padé approximations rician statistical functions," *IEEE Transactions on Aerospace and Electronic Systems*, AES-35, No. 4 (1999).
7. Eaves, J. L., and Reedy, E. K., *Principles of Modern Radar*, New York, NY: Van Nostrand Reinhold Company, Inc., 1987, ch. 11.
8. Goldman, J.,"Detection in the presence of spherically symmetric random vectors," *IEEE Transactions on Information Theory*, Vol. IT-22, No. 1, 52-59 (1976).
9. Goodman, N. R., "Statistical analysis based on a certain multivariate complex Gaussian distribution (an introduction)," *Annals of Mathematical Statistics*, 34, 152-180 (1963).
10. Lord, R. D., "The use of the Hankel transform in statistics," *Biometrika*, 41, 44-55 (1954).
11. Luke, Y. L., *Integrals of Bessel Functions*, McGraw-Hill, Inc., New York, NY, 1962, ch. 2.
12. Mitchell, R. L., and Walker, J. F., "Recursive methods for computing detection probabilities," *IEEE Transactions on Aerospace and Electronic Systems*, AES-7, No. 4, 671-676 (1971).
13. Rangaswamy, M., Weiner, D., and Öztürk, A., "Non-gaussian random vector identification using spherically invariant random processes," *IEEE Transactions on Aerospace and Electronic Systems*, Vol. 29, No. 1, 111-124 (1993).
14. Sangston, K. J. and Gerlach, K. R., "Non-gaussian noise models and coherent detection of radar targets," NRL Report 5341-92-9367, November 1992.
15. Sangston, K. J. and Gerlach, K. R., "Coherent detection of radar targets in a non-gaussian background," *IEEE Transactions on Aerospace and Electronic Systems*, Vol. 30, No. 2, 330-340 (1994).
16. Trunk, G. V., "Radar properties of non-Rayleigh sea clutter," *The IEEE Transactions on Aerospace and Electronic Systems*, AES-8, No. 2, 196-204 (1972).
17. Turin, G. L., "The characteristic function of Hermitian quadratic forms in complex normal variables," *Biometrika*, 47, 199-201 (1960).
18. Watson, G.N., *A Treaties on the Theory of Bessel Functions, Second Edition*, Cambridge University Press, Cambridge, England, 1944.
19. Wooding, R. A., "The multivariate distribution of complex normal random variables," *Biometrika*, 43, 212-215 (1956).
20. Yao, K., "A representation theorem and its applications to spherically-invariant random processes," *IEEE Transactions on Information Theory*, Vol. IT-19, No. 5, 600-608 (1973).

This page intentionally left blank.

Appendix A

THE COVARIANCE MATRIX FOR ECHOLOCATION PROBLEMS

When two or more complex matched filter outputs are used to detect a target, it is possible that an identical phase shift can appear across all the of the outputs. That is, if the k-th matched filter output $u_k + jv_k$ then

$$u_k + jv_k \rightarrow (u_k + jv_k)\exp(j\psi) = [u_k\cos(\psi) - v_k\sin(\psi)] + j[u_k\sin(\psi) + v_k\cos(\psi)]. \tag{A1}$$

This can occur in the following situations:

- If observations are obtained from a single matched filter output that is sampled in range delay or is sampled at the same range delay over several pings, a common phase shift can appear in all the observations if the target exhibits a slight change of range (smaller than a resolution cell) between scans[6].
- In frequency diversity system where observations are drawn simultaneously form several different frequency bands, slight changes in target range (again, between scans) will induce a phase change that will be nearly the same across all frequency bands if the percent difference between the largest and smallest band carrier frequency is small.
- If observations are drawn from a compact set of cells in the range-azimuth display, then a small, common shift in the steered beam directions (through reprocessing of the echoes) will induce an identical phase shift in the values of the sampled matched filter outputs.

In all of these situations, it is reasonable to assume that the statistical nature of the matched filter outputs do not significantly change, the result being that the correlation matrices, $\mathbf{P}$ and $\mathbf{R}$ as defined in Section 3.2, do not change. This is a generalization of the assumed circular symmetry of the joint PDF of the real and imaginary parts of the individual complex matched filter output.

From (A1), the invariance of the correlation matrix under the abovementioned phase shift implies that

$$\begin{bmatrix} E\{u_iu_k\} & E\{u_iv_k\} \\ E\{v_iu_k\} & E\{v_iv_k\} \end{bmatrix} = \begin{bmatrix} A & B \\ C & D \end{bmatrix} \tag{A2}$$

where

$$A = E\{u_iu_k\}\cos^2(\psi) + E\{v_iv_k\}\sin^2(\psi) - (E\{u_iv_k\} + E\{v_iu_k\})\cos(\psi)\sin(\psi) \tag{A3}$$
$$B = E\{u_iv_k\}\cos^2(\psi) - E\{v_iu_k\}\sin^2(\psi) + (E\{u_iu_k\} - E\{v_iv_k\})\cos(\psi)\sin(\psi) \tag{A4}$$
$$C = E\{v_iu_k\}\cos^2(\psi) - E\{u_iv_k\}\sin^2(\psi) + (E\{u_iu_k\} - E\{v_iv_k\})\cos(\psi)\sin(\psi) \tag{A5}$$
$$D = E\{v_iv_k\}\cos^2(\psi) + E\{u_iu_k\}\sin^2(\psi) + (E\{u_iv_k\} + E\{v_iu_k\})\cos(\psi)\sin(\psi). \tag{A6}$$

[6]In radar parlance, a "scan" refers to a collection of observations taken within a period of time when the target is within the antenna beam. Within a scan the target may be regarded as being stationary in range.

These equations can be expressed in the following matrix form:

$$\begin{bmatrix} \cos^2(\psi)-1 & -\cos(\psi)\sin(\psi) & -\cos(\psi)\sin(\psi) & \sin^2(\psi) \\ \cos(\psi)\sin(\psi) & \cos^2(\psi)-1 & -\sin^2(\psi) & -\cos(\psi)\sin(\psi) \\ \cos(\psi)\sin(\psi) & -\sin^2(\psi) & \cos^2(\psi)-1 & -\cos(\psi)\sin(\psi) \\ \sin^2(\psi) & \cos(\psi)\sin(\psi) & \cos(\psi)\sin(\psi) & \cos^2(\psi)-1 \end{bmatrix} \begin{bmatrix} A \\ B \\ C \\ D \end{bmatrix} = \begin{bmatrix} 0 \\ 0 \\ 0 \\ 0 \end{bmatrix}. \quad \text{(A7)}$$

This system of equations can be simplified by adding the first row to the last, subtracting the second row from the third, and multiplying the second row by $\cos(\psi)/\sin(\psi)$ and adding the result to the first row. The resulting reduced set of equations are

$$\begin{bmatrix} -1 & 0 & 0 & 1 \\ \cos^2(\psi) & -\cos(\psi)\sin(\psi) & -\cos(\psi)\sin(\psi) & -\cos^2(\psi) \end{bmatrix} \begin{bmatrix} A \\ B \\ C \\ D \end{bmatrix} = \begin{bmatrix} 0 \\ 0 \\ 0 \\ 0 \end{bmatrix}. \quad \text{(A8)}$$

The first row of (A8) implies that $A = D$. Substituting this result back into the second line of (A8) implies that $B = -C$. Therefore,

$$\begin{bmatrix} E\{u_i u_k\} & E\{u_i v_k\} \\ E\{v_i u_k\} & E\{v_i v_k\} \end{bmatrix} = \begin{bmatrix} A & -C \\ C & A \end{bmatrix}. \quad \text{(A9)}$$

This proves the form of the covariance sub-matrices defined in (60).

Appendix B

THE EXPECTED POWER FROM PADÉ APPROXIMATIONS TO THE CHARACTERISTIC FUNCTION

In this appendix it is shown that the expected power of a fluctuation model for $N_d = 1$ (single observation) can be calculated from the coefficients and poles of the Padé approximation to the CF that is given by (Sections 2.1 and 2.3)

$$\Phi(\rho) = 1 - \frac{E\{r^2\}}{4}\rho^2 + o(\rho^4) \approx \sum_{k=1}^{M} \frac{A_k}{(\rho^2 - p_k)^{m_k}} \tag{B1}$$

where r is the amplitude of the matched filter output defined in (1). It is easy to show that

$$\frac{1}{(\rho^2 - p_k)^{m_k}} = \frac{1}{(-p_k)^{m_k}} - \frac{m_k \rho^2}{(-p_k)^{m_k+1}} + o(\rho^4). \tag{B2}$$

Substituting (B2) into (B1) and grouping the coefficients for each power of ρ reveals that

$$E\{r^2 | N_d = 1\} = 4 \sum_{k=1}^{M} \frac{m_k A_k}{(-p_k)^{m_k+1}} = 4\eta \tag{B3}$$

where η is the normalization coefficient defined in Section 3.5. This formula is always exact if moment matching is used to find the coefficients of the Padé approximation in (B1). This is because the second moment of the amplitude PDF is always used in the matrix equations describing the Padé coefficients ((10) through (12) in Section 2.3).